Interpreting the ultraviolet absorption in the spectrum of 415 nm-bandgap CdSe magic-size clusters

Zhu, Dikai; Hui, Juan; Rowell, Nelson; Liu, Yuanyuan; Chen, Queena Y.; Steegemans, Tristan; Fan, Hongsong; Zhang, Meng; Yu, Kui

Publisher's version / Version de l'éditeur:
https://doi.org/10.1021/acs.jpclett.8b01109
The Journal of Physical Chemistry Letters, 9, 11, pp. 2818-2824, 2018-05-15

THE JOURNAL OF PHYSICAL CHEMISTRY Letters

Cite This: J. Phys. Chem. Lett. 2018, 9, 2818−2824

Letter

pubs.acs.org/JPCL

Interpreting the Ultraviolet Absorption in the Spectrum of 415 nm-Bandgap CdSe Magic-Size Clusters

Dikai Zhu,[†] Juan Hui,[†] Nelson Rowell,[‡] Yuanyuan Liu,[†] Queena Y. Chen,[‡] Tristan Steegemans,[†] Hongsong Fan,[§] Meng Zhang,*[,†] and Kui Yu*[,†,§,∥]

[†]Institute of Atomic and Molecular Physics, Sichuan University, Chengdu 610065, People's Republic of China

[‡]National Research Council Canada, Ottawa, Ontario K1A 0R6, Canada

[§]Engineering Research Center in Biomaterials, Sichuan University, Chengdu 610065, People's Republic of China

[∥]Chemical Engineering, Sichuan University, Chengdu 610065, People's Republic of China

Supporting Information

ABSTRACT: Colloidal semiconductor magic-size clusters (MSCs), a crucial link between molecular and bulk materials, have attracted attention in the past three decades. However, the identification of their nonbandgap electronic transitions via optical absorption has been challenging due to the possible presence of other-bandgap ensembles in synthetic batches. For CdSe MSC-415, referred to as the optical absorption ($1S(e)-1S_{3/2}(h)$) in nanometers of wavelength, we report our exploration on the origin of two commonly documented absorption peaks at 381 and 351 nm. We show that the evolution of the two peaks does not synchronize with that of the ∼415 nm peak and seems to be respectively related to the disappearance of MSC-391 and MSC-361. Accordingly, these two peaks detected are probably not due to higher order electronic transitions in MSC-415. The present study shows the necessity of re-evaluating previous experimental results and of developing advanced theoretical models to better understand the quantized energy levels of MSCs.

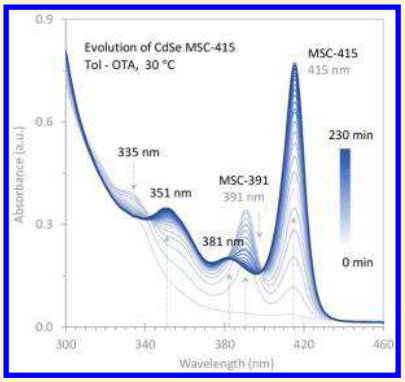

Cluster science aims at bridging the knowledge gap of the change in fundamental properties as the number of atoms evolving from individual molecules to condensed-phase matter.[1,2] Various fullerene,[3,4] metal, and noble metal clusters[5−14] have been documented, together with semiconductor clusters.[15−29] The term "magic-number" or "magic-size"[3−28] has been used to describe those with enhanced stability. The origin of the magic stability has been attributed to both full shells of electrons and geometric structures.[7−10,15]

Magic-size clusters (MSCs) have been used by the semiconductor research community.[15−28] For the research of colloidal semiconductor nanocrystals (NCs), a large portion of interest has been directed toward potential applications in a number of areas including bioimaging,[30,31] light emitting diodes (LED),[32,33] and solar cells.[34,35] These studies have generally employed conventional quantum dots (QDs) rather than MSCs. For one given semiconductor NC ensemble, the size distribution and thus the optical bandwidth of the conventional QDs are larger than that of the MSCs. Although current research into semiconductor clusters is not as advanced as that for the other cluster materials,[3−14] various synthetic approaches have been reported since 1993 to obtain sp^3-hybridization semiconductor CdSe MSC-415.[15−23,36,37] The MSCs are here referenced by their bandgap energy in wavelength (415 nm), corresponding to the lowest allowed electronic transition ($1S(e)-1S_{3/2}(h)$).[36−38]

For the CdSe MSC-415 ensembles reported,[15−23] their syntheses were performed in aqueous[15−17] or organic solutions,[18−23] with phosphine/phosphine oxide,[18,23] phosphinate,[19] carboxylate,[21] or amines[15,20−22] as surface ligands. Details of the synthetic conditions are summarized in Table S1. In addition to the bandgap absorption peak at 414 to 422 nm, interestingly, another two absorption peaks in the range from 382 to 398 nm and from 352 to 365 nm have been often reported. It seems reasonable that the variation in these absorption peak positions could be due to experimental conditions. For the two shorter-wavelength peaks, their absorbance is much weaker, and they have been generally taken respectively as due to the secondary and third electronic transitions of MSC-415. However, the assignment would appear to be questionable.[15−23]

To explore the origin of the two out-of-band absorption peaks for MSC-415, it is important to have experimental data to demonstrate that the MSC-415 ensembles produced consist of no other-bandgap NCs. Only when MSC-415 is produced in a single-bandgap form can the two out-of-band absorption peaks be due to the secondary and third electronic transitions. On the other hand, if the MSC-415 ensemble produced contains other-bandgap NCs, the two accompanying absorption peaks may not

Received: April 10, 2018
Accepted: May 11, 2018
Published: May 15, 2018

DOI: 10.1021/acs.jpclett.8b01109
J. Phys. Chem. Lett. 2018, 9, 2818−2824

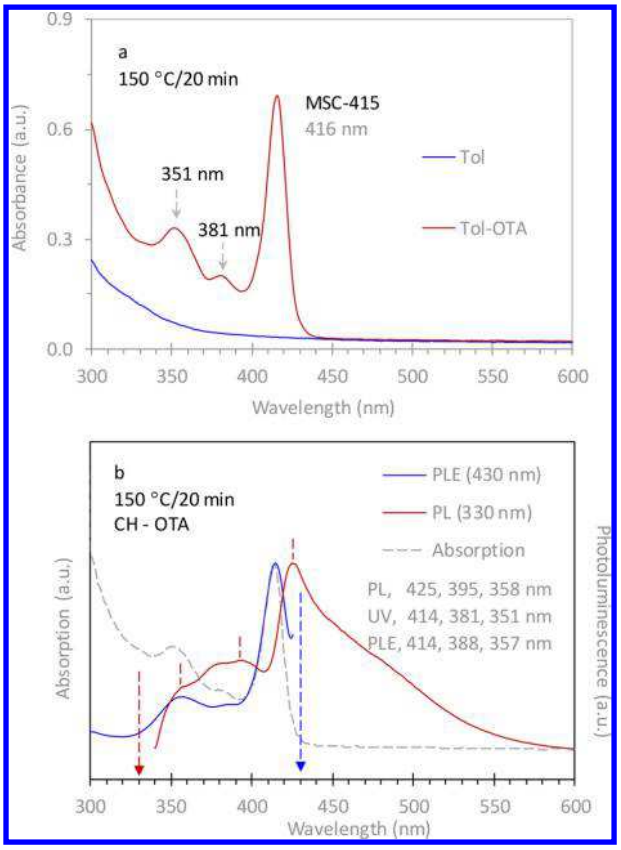

Figure 1. Optical spectroscopy of one CdSe sample extracted from a reaction batch of $Cd(OAc)_2$/OLA + SeTOP at 150 °C with a growth period of 20 min. (a) Absorption spectra of the sample (300 μL) in 3.0 mL of Tol (blue trace) and in the mixture of 2.0 mL Tol and 1.0 mL OTA mixture (red trace). (b) Normalized absorption (gray dashed trace), emission (red trace, with excitation wavelength of 330 nm), and excitation (blue trace, with emission wavelength of 430 nm) spectra of the sample (30 μL) in the mixture of 2.0 mL cyclohexane (CH) and 1.0 mL OTA at RT.

be unambiguously assigned to the secondary and third electronic transitions.

Herein, we report our exploration on the origin of the two absorption peaks at ~381 and ~351 nm for CdSe MSC-415. We used a two-step approach to decouple the evolution of CdSe MSC-415 from the formation of precursor samples, which are transparent in optical absorption. With cadmium acetate $Cd(OAc)_2$ and selenium (Se) powder as Cd and Se sources, respectively, the first step was conducted in oleylamine (OLA) at 150 °C to prepare a transparent sample in optical absorption. The Cd and Se precursors were respectively $Cd(OAc)_2$/OLA and tri-*n*-octylphosphine selenide (SeTOP). The reaction products were explored by electrospray ionization mass spectrometry (ESI-MS) to evaluate the formation of Cd and Se covalent bonds when the reaction temperature was increased. The second step was mainly carried out in a mixture of toluene (Tol) and octylamine (OTA) at a lower temperature, with the detailed evolution of MSCs *in situ* monitored by absorption spectroscopy. We show that the evolution of MSCs does not seem to be in agreement with the literature assignment that the weak absorption peaks at ~381 and ~351 nm were due to the higher order electronic transitions in MSC-415.[21,22] It seems more likely that they are respectively related to the disappearance of MSC-391 and MSC-361. The present study suggests that further developments are needed, with regard to synthesis, characterization, and theoretical modeling, to attain a better understanding of the electronic structures of semiconductor MSCs.

Figure 1a shows the optical absorption spectra collected from a CdSe sample extracted from the reaction at 150 °C and a growth duration of 20 min. An aliquot (300 μL) of the sample was dispersed into 3.0 mL Tol (blue trace) and into a mixture of 2.0 mL Tol and 1.0 mL OTA (red trace) at 50 °C. The spectra were collected after being dispersed for 5 min. Among the six samples with the growth periods of 0, 20, 30, 40, 50, and 60 min (as shown in Figure S1−1), the 150 °C/20 min sample exhibits the highest optical density at 416 nm in the Tol-OTA mixture without the presence of conventional quantum dots (QDs).

The absorption spectrum of MSC-415 obtained with the two out-of-band peaks at 381 and 351 nm is similar to those spectra previously reported.[15−23] For the sample dispersed in a mixture

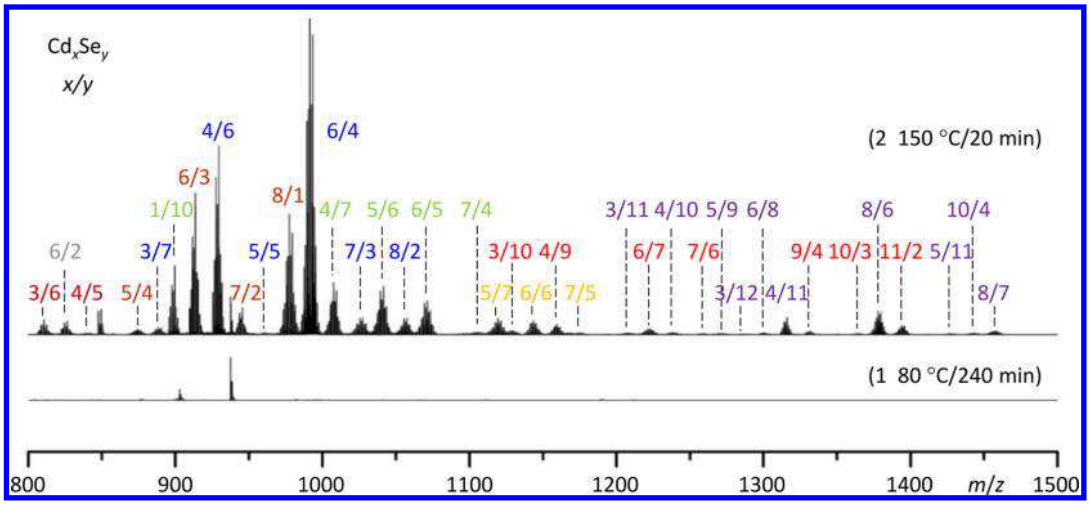

Figure 2. ESI-MS spectra of two samples from two reactions of $Cd(OAc)_2$/OLA + SeTOP, 80 °C/240 min (1) and 150 °C/20 min (2). Figure S2−1 shows the corresponding optical absorption spectra of Sample 1 (but from a different batch). Sample 2 was obtained from another batch identical to that of Figure 1. CdSe MSCs were not detected in Sample 1 but were in Sample 2 in the Tol−OTA mixture. The presence of the Cd_xSe_y fragments in Sample 2 can be attributed to the formation of Cd and Se covalent bonds.

DOI: 10.1021/acs.jpclett.8b01109
J. Phys. Chem. Lett. 2018, 9, 2818−2824

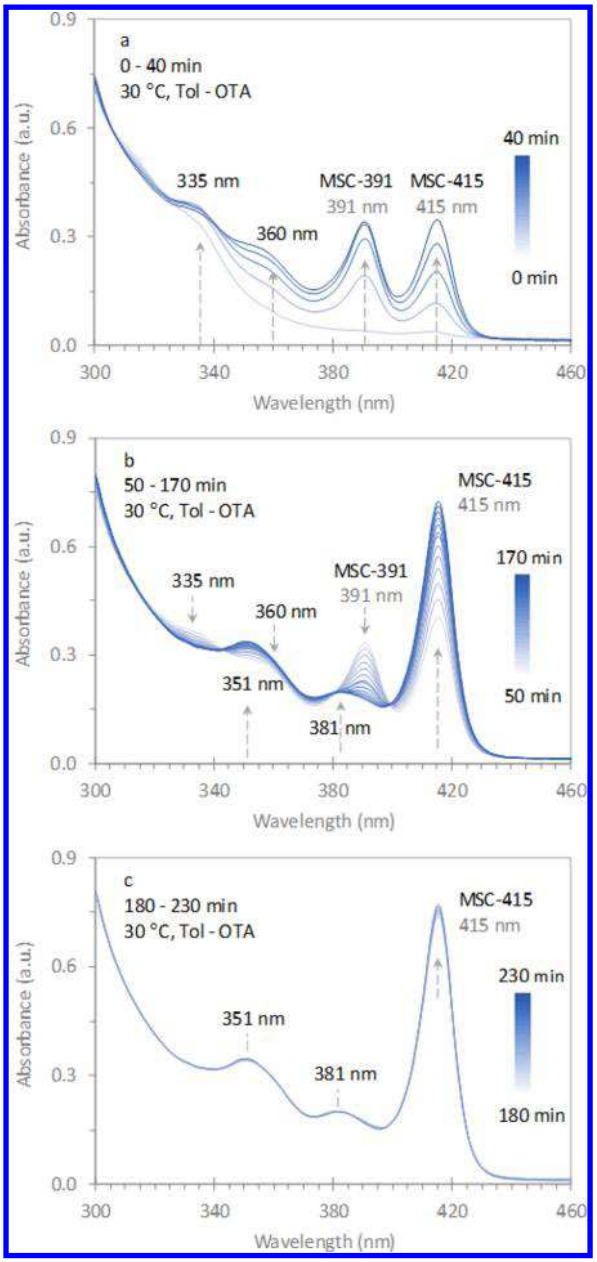

Figure 3. *In situ* absorption spectra collected from one dispersion at 30 °C with a time interval of 10 min. The dispersion was made from one 150 °C/20 min sample (300 μL) in a mixture of 1.8 mL Tol and 1.2 mL OTA at 30 °C. The spectra are presented in parts a (0−40 min), b (50−170 min), and c (180−230 min). CdSe MSC-391 and MSC-415 formed (a). MSC-391 started to disappear after 50 min, and a new peak at 381 nm formed gradually along with the disappearance of MSC-391 (b). MSC-415 kept accumulating and reached a plateau eventually, with little change for the 381 and 351 nm peaks (b and c).

of cyclohexane (CH) and OTA, we explored further with photoluminescence emission (PL, red trace) and excitation (PLE, blue trace) as shown in Figure 1b, together with the absorption spectrum (dashed gray trace). Upon 330 nm excitation (red trace), the dispersion exhibited emission peaking at 425, 395, and 358 nm. For 430 nm emission (blue trace), the dispersion displayed PLE peaking at 414 nm. Thus, the 425 nm PL appears to be the bandgap emission of MSC-415, for which the bandgap absorption peak is at 414 nm. It is noteworthy that excited with wavelength shorter than that of bandgap, conventional QDs exhibit bandgap and/or trap PL, without higher order transition emission. At the same time, for a special type of CdSe NCs that exhibit one sharp absorption doublet, only bandgap (and no higher order transition) emission was detected.[39−41] Therefore, the appearance of PL peaking at 395 and 360 nm is consistent with the presence of other-bandgap NCs in the dispersion. Accordingly, the two accompanying absorption peaks at 381 and 351 nm would not be related to the higher order electronic transitions of MSC-415. As a side note, the bandgap emission detected is similar to that reported elsewhere.[16]

The synthesis of CdSe MSC-415, producing the Figure 1a red trace absorption, was via our two-step approach. The first step was the formation of a transparent sample (Figure 1a blue trace) in the reaction of $Cd(OAc)_2$/OLA and SeTOP at 150 °C for ∼20 min, and the second step was the growth of MSCs from the first-step sample in the Tol-OTA mixture at 50 °C. The 150 °C/20 min samples from repeated batches were used in the following study (Figures 2−5). (Absorption results for other condition samples are shown in Figures S1-1, S1-3, and S1-4).

For the first-step reaction samples, ESI-MS was used to monitor the formation of Cd−Se covalent bonds. Figure 2 shows ESI-MS spectra (with a positive-ion mode within the m/z range from 800 to 1500 Da) of two samples from two $Cd(OAc)_2$/OLA + SeTOP reaction batches at 80 °C (trace 1) and 150 °C (trace 2). The growth periods were 240 and 20 min, respectively. For the 80 °C sample (trace 1), no fragments of the Cd_xSe_y form were detected. The two peaks in the m/z range of 900 to 950 Da were from the Cd precursor.[24] Figure S2-1 shows that this sample in both Tol and the Tol-OTA mixture is transparent in optical absorption. For the 150 °C sample (trace 2), cluster fragments of Cd_xSe_y were detected. ESI-MS has been used to characterize reaction intermediates of semiconductor II−VI NCs,[24,25] and the cluster fragments detected were free of surface ligands.[24−27] Based on the Cd and Se isotopic patterns (Figure S2-2), the compositions of Cd_xSe_y fragments are assigned with the integer values indicated for x and y. The fragmented 9- to 16-atom clusters were apparently detected, with two 10-atom clusters, Cd_6Se_4 and Cd_4Se_6, occurring most often. Large fragments in the m/z range of 1200−1500 Da had relatively weak peaks. Figure S2-3 presents the expanded views of the cluster fragments detected from this sample. Both Figures 2 and S2 demonstrate that Cd−Se covalent bonds formed for the 150 °C sample, but not for the 80 °C sample. Thus, for our decoupled two-step approach, the first step was carried out at 150 °C to prepare IPs, while the second step was to obtain MSCs at lower temperatures from the preheated IP. As illustrated below, the second step was performed at 30 °C (Figure 3) and in the temperature range of 10−60 °C (Figure 4).

Figure 3 presents the evolution of MSC-415 via the temporal variation of the absorption of the first-step 150 °C/20 min sample (300 μL) in a mixture of Tol (1.8 mL) and OTA (1.2 mL) at 30 °C. The use of 30 °C was due to the fact that the evolution of MSC-415 at 50 °C reached a high optical density in just 5 min (Figure 1a, red trace). The absorption spectra were recorded every 10 min. The evolution in the second step at 30 °C seemed to involve three phases, from 0 to 40 min (3a), 50 to 170 min (3b), and 180 to 230 min (3c). Figure S3-1 shows the whole temporal evolution 0 to 230 min (a), 0 to 30 min (b), and 40 to 230 min (c). Figure S3-2 presents the evolution at 30 °C of the sample dispersed in Tol, OTA, and

DOI: 10.1021/acs.jpclett.8b01109
J. Phys. Chem. Lett. 2018, 9, 2818−2824

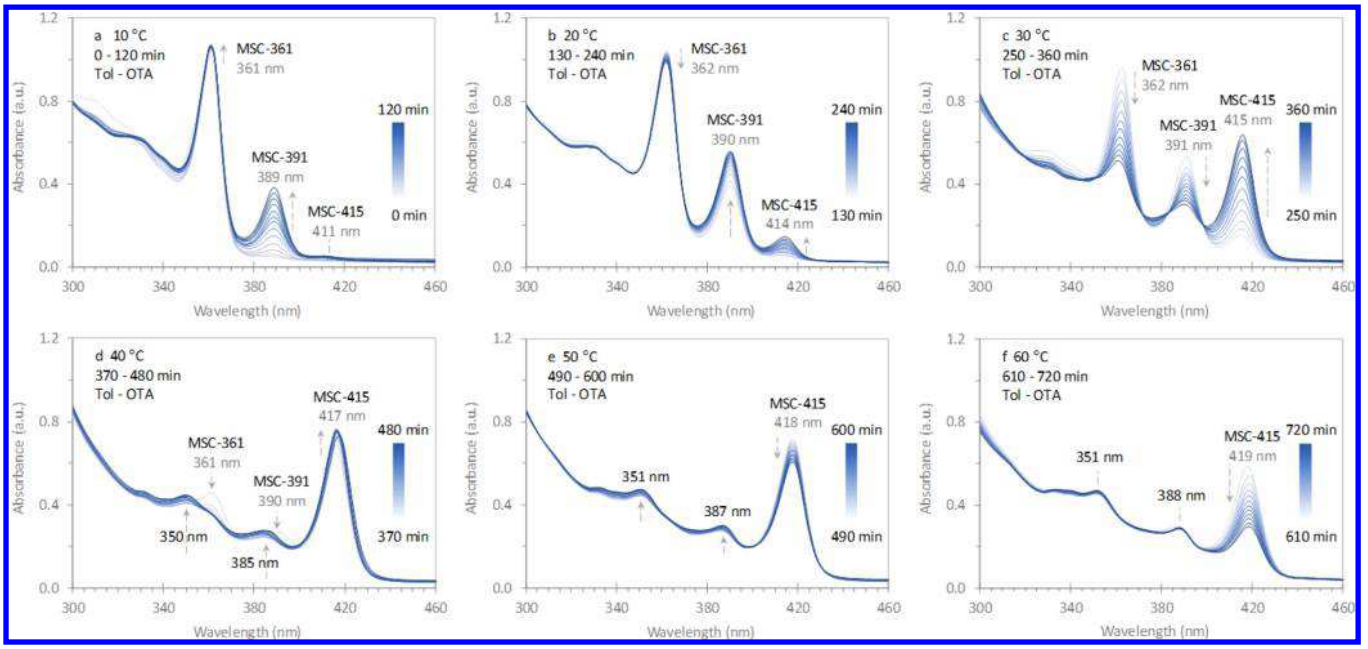

Figure 4. *In-situ* absorption spectra collected from one dispersion with the 10 °C step from 10 to 60 °C. 120 min was maintained at each temperature, and the spectra were recorded every 10 min. The dispersion was made from one 150 °C/20 min sample (300 μL) in a mixture of 1.8 mL Tol and 1.2 mL OTA. Before the measurements, the dispersion was stored at −25 °C for 48 h. Interestingly, MSC-361 and MSC-391 were detected (a−c), but disappeared (d and f) accompanied by the presence of 351 and 381 nm peaks, respectively. MSC-415 kept accumulating and reached a plateau eventually (a−d), and started to decrease (e and f) with little change for the 381 and 351 nm peaks (f).

their mixtures of four volume ratios. For the 415 nm peak, we observed a continuous increase in its optical density throughout the whole evolution progress from 0 to 230 min (Figures 3 and S3-1). However, the two shorter wavelength 381 and 351 nm peaks did not. Certainly the three peaks did not exhibit a synchronized evolution behavior.

In the initial stage from 0 to 40 min (3a), the two peaks at 391 and 415 nm appeared, together with a 360 nm peak. The peaks at 381 and 351 nm were not present. From 50 to 170 min (2b), the strength of the peak at 391 nm decreased. As the peak at 391 nm almost disappeared, a peak at 381 nm developed. At the same time, a similar trend was observed for the peak at 360 nm, which disappeared while a new peak at 351 nm emerged. A typical MSC-415 spectrum was obtained at 170 min, which is similar to that of the red trace of Figure 1a. From 180 to 230 min (3c), the intensity of the 415 nm peak increased slightly, and that of the two peaks at 381 and 351 nm changed little. The absence of correlation between the intensity variations indicates that these two peaks are not coming from MSC-415. Figures 3 and S3 present strong experimental evidence that these two peaks at 381 and 351 nm do not result from the higher order electronic transitions in MSC-415.

Up to this point, we have explored the evolution of MSCs at a constant temperature of 30 °C. Figure 4 shows the evolution of MSCs monitored when the temperature was increased from 10 to 60 °C. The evolution was allowed to run for 120 min at each 10 °C step, and the absorption spectra were collected *in situ* with a 10 min interval. Before the measurement, the dispersion was stored at −25 °C for 48 h. Interestingly, the evolution of MSC-391 and MSC-361 occurred prior to that of MSC-415 (4a). Along the disappearance of MSC-391 and MSC-361 (4c and 4d), the two weak peaks at 381 and 351 nm developed, respectively. These two peaks changed little while the 415 nm peak decreased in intensity (4e and 4f).

At 10 °C (Figure 4a), the absorption peaking at 361 nm changed little, suggesting that the population of MSC-361 was constant. When the temperature was increased to 20 and 30 °C (4b and 4c), the 361 nm peak started to decline, and was completely gone at 40 °C (4d); meanwhile, a new peak at 350 nm appeared. Such a variation is similar to that observed at the constant temperature of 30 °C (Figure 3b). MSC-391 developed also at 10 °C (4a); its population apparently reached maximum at 20 °C (4b), decreased at 30 °C (4c), and became negligibly at 40 °C (4d); at the same time, a new peak at 385 nm was observed (4d). Again, this behavior is similar to what seen at 30 °C (Figure 3b). The absorption peak corresponding to MSC-415 started to be visible at 10 °C (4a), and reached its strongest strength at 40 °C and became dominant peaking at 417 nm (4d).

At 50 °C (Figure 4e), the MSC-415 bandgap absorption peak shifted to 418 nm with slightly decreased intensity; meanwhile, for the other two peaks that shifted to 387 and 351 nm, their intensity exhibited a small but appreciable increase. At 60 °C (4f), the MSC-415 bandgap absorption peak shifted further to 419 nm with significant decrease in intensity, while the two accompanying 388 and 351 nm peaks changed little. Evidently, the absorption peak red-shifted when the temperature was increased from 40 to 60 °C; the 351 nm peak seems to be less sensitive. Critically, the intensity of the absorption peak at 419 nm decreased by ∼60% in 120 min at 60 °C, but the two peaks at 388 and 351 nm remained unchanged in strength (4f). The ∼381 and ∼351 nm peaks respectively appeared only when the MSC-391 and MSC-361 peaks vanished (Figure 3 and Figures 4a−d).

Figure S4-1 shows the temporal evolution of absorption from the CdSe sample in various Tol-OTA mixtures at 60 °C. Figure S4-2 presents the absorption evolution of the CdSe sample in two Tol-OTA mixtures at 5 °C (after being stored at −25 °C for 24 h). The results provide further experimental evidence

DOI: 10.1021/acs.jpclett.8b01109
J. Phys. Chem. Lett. 2018, 9, 2818−2824

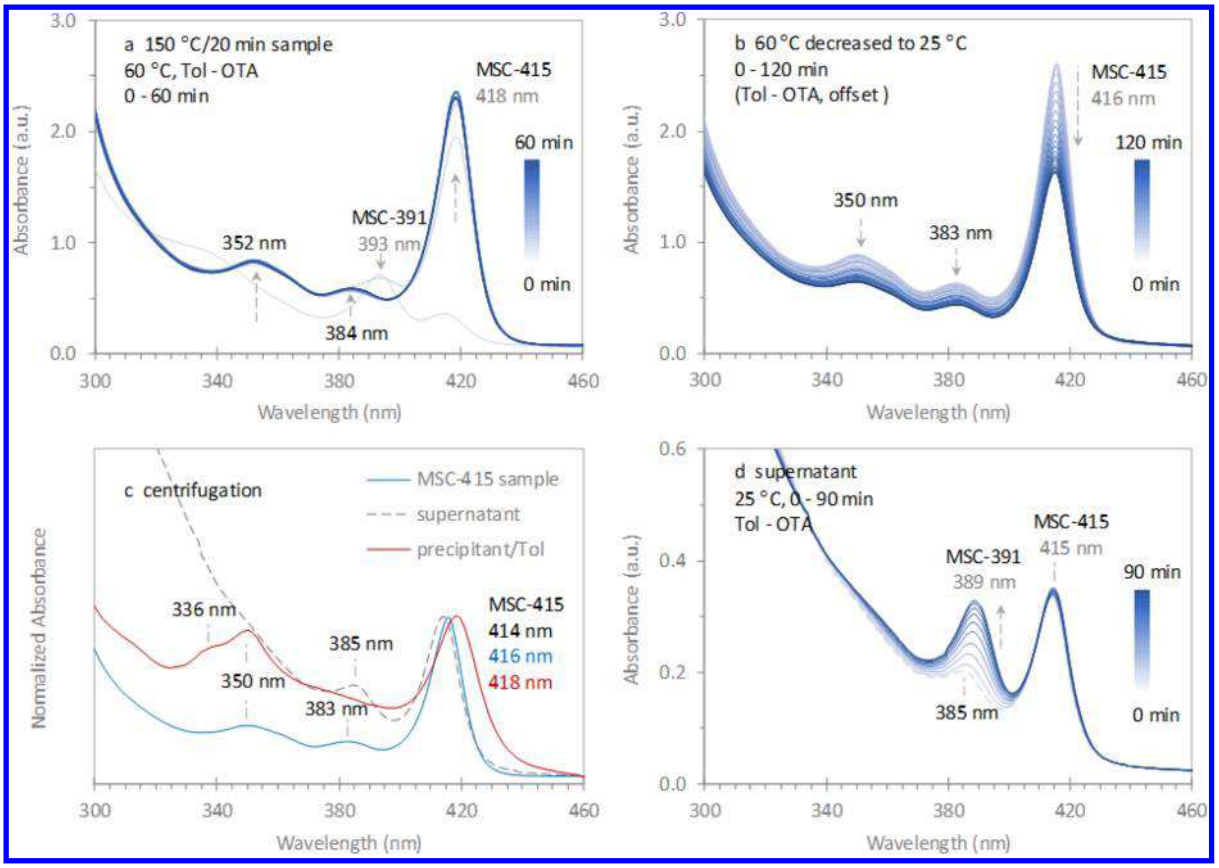

Figure 5. Centrifugation-assisted exploration with absorption spectroscopy. (a) Preparation of one MSC-415 dispersion at 60 °C for 60 min. One 150 °C/20 min sample (1.0 mL) was dispersed in a mixture of 1.0 mL Tol and 4.0 mL OTA at 60 °C. (b) The 60 min dispersion (a) was cooled down to 25 °C and monitored for 120 min. Clearly, the intensity of the three peaks progressively became weaker, with more decrease for MSC-415. (c) The dispersion (a) was centrifuged. Spectra were collected for the 60 min dispersion (a) before centrifugation (blue trace), the supernatant after 30 min centrifugation (dashed gray trace), and the precipitate (after 5 min centrifugation and dispersed in Tol, red trace). The three spectra were normalized according to the ~415 nm peak absorbance. (d) The spectra of the supernatant monitored for 90 min. Critically, the 385 nm peak gradually intensified and red-shifted; however, the 415 nm peak changed little.

that the two accompanying peaks at 381 and 351 nm in the absorption spectrum of MSC-415 are not associated with higher order electronic transition processes in MSC-415.

Figure 5 contains the results of our optical absorption study of a well-developed CdSe MSC-415 dispersion sample (a), when its temperature was decreased to 25 °C (room temperature) (b), and after centrifugation at 25 °C (c and d). It is worthy of notice that this sample did not contain any conventional QDs. Centrifugation is often used to purify colloidal semiconductor NCs.[18,22] For the first-step sample in the mixture of Tol and OTA at 60 °C, Figure 5a shows the temporal evolution of absorption up to 1 h (with spectra collected each 10 min). After 20 min, a typical MSC-415 spectrum developed (with the apparent bandgap absorption peaking at 418 nm and two accompanying blue-side weak peaks at 384 and 352 nm). For the 60 min MSC dispersion, a portion was cooled to 25 °C, and Figure 5b shows the temporal evolution of absorption at 25 °C; the spectra were collected every 10 min and are displayed with offset; the original spectra are shown in Figure S5. The three peaks of interest shifted to 416, 383, and 350 nm at 25 °C.

At the same time, the rest of the 60 min MSC dispersion (a) was centrifuged at 9000 rpm (at 25 °C). Absorption measurements (Figure 5c) were performed for the sample before centrifugation (blue trace), the resulting supernatant (with 30 min centrifugation, dashed gray trace), and the precipitate (with 5 min centrifugation, in Tol, red trace). The spectra are normalized (for the ~415 nm peaks). Evidently, the blue and red traces do not match exactly. The starting dispersion (blue trace) exhibited a main peak at 416 nm and two additional small peaks at 383 and 350 nm. The precipitate (red trace) exhibited a dominant peak at 418 nm and one weaker peak at 350 nm. The supernatant (dashed gray trace) displayed a main peak at 414 nm and a small peak at 385 nm.

Figure 5d shows the temporal evolution of absorption for the supernatant at 25 °C with spectra collected every 10 min. The 385 nm peak gradually increased in intensity and shifted to 389 nm, which might suggest the presence of MSC-391. The intensification of this peak might be due to the possible existence of the CdSe IP. Meanwhile, the 415 nm peak intensity changed little. A salient point, here, is that the evolution patterns of the ~415 and ~385 nm peaks are quite different at 25 °C, as shown in Figure 5b,d. The results shown in Figure 5 strongly support our hypothesis that the two accompanying peaks in the spectrum of MSC-415 are not due to the higher-order electronic transitions.

In conclusion, we have explored the origin of the two out-of-band absorption peaks at 381 and 351 nm in the absorption spectrum of CdSe MSC-415. The two shorter wavelength peaks have been observed numerous times in the absorption spectra from CdSe MSC-415 samples.[15−23] We have monitored the evolution of MSC-415 via absorption spectroscopy (Figures 3

DOI: 10.1021/acs.jpclett.8b01109
J. Phys. Chem. Lett. 2018, 9, 2818−2824

and 4), using a sample that was preheated at 150 °C for 20 min to result in the formation of Cd−Se covalent bonds in the first step, and which was transparent in optical absorption (Figures 1 and 2). The absorption spectrum of MSC-415 from our two-step approach also exhibited a sharp absorption peak at ∼415 nm, with two accompanying peaks at ∼381 and ∼351 nm. The evolution of MSC-415 was sensitive to the nature of the dispersion solvent and the temperature used (in the second step). The two accompanying peaks exhibited different evolution behaviors, as compared to that of MSC-415; they only appeared after the disappearance of MSC-391 and MSC-361 (Figures 3 and 4). The absorption of the supernatant (obtained from a MSC-415 dispersion) exhibited the increase of MSC-391, with MSC-415 displaying relatively constant peak strength at ∼415 nm (Figure 5). The present study suggests that the two peaks at 381 and 351 nm in the MSC-415 absorption spectrum are probably not due to the higher order electronic transitions in MSC-415. Efforts such as two-dimensional PLE measurements at low temperature will be considered in the near future. Our findings indicate that a challenge remains with regard to synthesizing MSCs in a single ensemble form without the coexistence of other-bandgap species. Also, the present study calls for further efforts to explain what actually causes these two peaks, including theoretical modeling with regard to the relationship between structural and electronic properties in semiconductor MSCs.

■ ASSOCIATED CONTENT

Supporting Information

The Supporting Information is available free of charge on the ACS Publications website at DOI: 10.1021/acs.jpclett.8b01109.

Experimental details including synthesis and characterization, with literature summary and additional absorption and mass spectra (PDF)

■ AUTHOR INFORMATION

Corresponding Authors

*E-mail: mengzhang@scu.edu.cn.
*E-mail: kuiyu@scu.edu.cn.

ORCID

Hongsong Fan: 0000-0003-3812-9208
Kui Yu: 0000-0003-0349-2680

Notes

The authors declare no competing financial interest.

■ ACKNOWLEDGMENTS

K.Y. thanks the National Natural Science Foundation of China (NSFC) 21573155 and 21773162, and the Fundamental Research Funds for the Central Universities SCU2015A002. We thank Open Project of Key State Laboratory for Supramolecular Structures and Materials of Jilin University for SKLSSM 201830. We thank Dr. Mingdong Liu for our MS measurements in National Institute of Measurement and Testing Technology in Chengdu.

■ REFERENCES

(1) Alivisatos, A. P. Semiconductor Clusters, Nanocrystals, and Quantum Dots. *Science* **1996**, *271*, 933−937.
(2) Castleman, A. W.; Bowen, K. H. Clusters: Structure, Energetics, and Dynamics of Intermediate States of Matter. *J. Phys. Chem.* **1996**, *100*, 12911−12944.
(3) Kroto, H. W.; Heath, J. R.; O'Brien, S. C.; Curl, R. F.; Smalley, R. E. C_{60}: Buckminsterfullerene. *Nature* **1985**, *318*, 162−163.
(4) Krätschmer, W.; Lamb, L. D.; Fostiropoulos, K.; Huffman, D. R. Solid C_{60}: A New Form of Carbon. *Nature* **1990**, *347*, 354−358.
(5) Robbins, E. J.; Leckenby, R. E.; Willis, P. The Ionization Potentials of Clustered Sodium Atoms. *Adv. Phys.* **1967**, *16*, 739−744.
(6) Brack, M. Metal Clusters and Magic Numbers. *Sci. Am.* **1997**, *277*, 50−55.
(7) Negishi, Y.; Takasugi, Y.; Sato, S.; Yao, H.; Kimura, K.; Tsukuda, T. Magic-Numbered Au_n Clusters Protected by Glutathione Monolayers (n = 18, 21, 25, 28, 32, 39): Isolation and Spectroscopic Characterization. *J. Am. Chem. Soc.* **2004**, *126*, 6518−6519.
(8) Negishi, Y.; Chaki, N. K.; Shichibu, Y.; Whetten, R. L.; Tsukuda, T. Origin of Magic Stability of Thiolated Gold Clusters: A Case Study on $Au_{25}(SC_6H_{13})_{18}$. *J. Am. Chem. Soc.* **2007**, *129*, 11322−11323.
(9) Negishi, Y.; Sakamoto, C.; Ohyama, T.; Tsukuda, T. Synthesis and the Origin of the Stability of Thiolate-Protected Au_{130} and Au_{187} Clusters. *J. Phys. Chem. Lett.* **2012**, *3*, 1624−1628.
(10) Copp, S. M.; Schultz, D.; Swasey, S.; Pavlovich, J.; Debord, M.; Chiu, A.; Olsson, K.; Gwinn, E. Magic Numbers in DNA-Stabilized Fluorescent Silver Clusters Lead to Magic Colors. *J. Phys. Chem. Lett.* **2014**, *5*, 959−963.
(11) Jose, D.; Matthiesen, J. E.; Parsons, C.; Sorensen, C. M.; Klabunde, K. J. Size Focusing of Nanoparticles by Thermodynamic Control through Ligand Interactions. Molecular Clusters Compared with Nanoparticles of Metals. *J. Phys. Chem. Lett.* **2012**, *3*, 885−890.
(12) Jin, R.; Zeng, C.; Zhou, M.; Chen, Y. Atomically Precise Colloidal Metal Nanoclusters and Nanoparticles: Fundamentals and Opportunities. *Chem. Rev.* **2016**, *116*, 10346−10413.
(13) Jensen, K. M.; Juhas, P.; Tofanelli, M. A.; Heinecke, C. L.; Vaughan, G.; Ackerson, C. J.; Billinge, S. J. Polymorphism in Magic-Sized $Au_{144}(SR)_{60}$ Clusters. *Nat. Commun.* **2016**, *7*, 11859.
(14) Shi, L.; Zhu, L.; Guo, J.; Zhang, L.; Shi, Y.; Zhang, Y.; Hou, K.; Zheng, Y.; Zhu, Y.; Lv, J.; Liu, S.; Tang, Z. Self-Assembly of Chiral Gold Clusters into Crystalline Nanocubes of Exceptional Optical Activity. *Angew. Chem., Int. Ed.* **2017**, *56*, 15397−15401.
(15) Kasuya, A.; Sivamohan, R.; Barnakov, Y. A.; Dmitruk, I. M.; Nirasawa, T.; Romanyuk, V. R.; Kumar, V.; Mamykin, S. V.; Tohji, K.; Jeyadevan, B.; Shinoda, K.; Kudo, T.; Terasaki, O.; Liu, Z.; Belosludov, R. V.; Sundararajan, V.; Kawazoe, Y. Ultra-Stable Nanoparticles of CdSe Revealed from Mass Spectrometry. *Nat. Mater.* **2004**, *3*, 99−102.
(16) Park, Y.-S.; Dmytruk, A.; Dmitruk, I.; Kasuya, A.; Okamoto, Y.; Kaji, N.; Tokeshi, M.; Baba, Y. Aqueous Phase Synthesized CdSe Nanoparticles with Well-Defined Numbers of Constituent Atoms. *J. Phys. Chem. C* **2010**, *114*, 18834−18840.
(17) Kurihara, T.; Noda, Y.; Takegoshi, K. Quantitative Solid-State NMR Study on Ligand-Surface Interaction in Cysteine-Capped CdSe Magic-Sized Clusters. *J. Phys. Chem. Lett.* **2017**, *8*, 2555−2559.
(18) Murray, C. B.; Norris, D. J.; Bawendi, M. G. Synthesis and Characterization of Nearly Monodisperse CdE (E = S, Se, Te) Semiconductor Nanocrystallites. *J. Am. Chem. Soc.* **1993**, *115*, 8706−8715.
(19) Dukes, A. D.; McBride, J. R.; Rosenthal, S. J. Synthesis of Magic-Sized CdSe and CdTe Nanocrystals with Diisooctylphosphinic Acid. *Chem. Mater.* **2010**, *22*, 6402−6408.
(20) Evans, C. M.; Love, A. M.; Weiss, E. A. Surfactant-Controlled Polymerization of Semiconductor Clusters to Quantum Dots through Competing Step-Growth and Living Chain-Growth Mechanisms. *J. Am. Chem. Soc.* **2012**, *134*, 17298−17305.
(21) Newton, J. C.; Ramasamy, K.; Mandal, M.; Joshi, G. K.; Kumbhar, A.; Sardar, R. Low-Temperature Synthesis of Magic-Sized CdSe Nanoclusters: Influence of Ligands on Nanocluster Growth and Photophysical Properties. *J. Phys. Chem. C* **2012**, *116*, 4380−4389.
(22) Dolai, S.; Nimmala, P. R.; Mandal, M.; Muhoberac, B. B.; Dria, K.; Dass, A.; Sardar, R. Isolation of Bright Blue Light-Emitting CdSe Nanocrystals with 6.5 kDa Core in Gram Scale: High Photoluminescence Efficiency Controlled by Surface Ligand Chemistry. *Chem. Mater.* **2014**, *26*, 1278−1285.

DOI: 10.1021/acs.jpclett.8b01109
J. Phys. Chem. Lett. 2018, 9, 2818−2824

(23) Yu, K.; Hu, M. Z.; Wang, R.; Piolet, M. l. L.; Frotey, M.; Zaman, M. B.; Wu, X.; Leek, D. M.; Tao, Y.; Wilkinson, D.; Li, C. Thermodynamic Equilibrium-Driven Formation of Single-Sized Nanocrystals: Reaction Media Tuning CdSe Magic-Sized versus Regular Quantum Dots. *J. Phys. Chem. C* **2010**, *114*, 3329−3339.
(24) Liu, M.; Wang, K.; Wang, L.; Han, S.; Fan, H.; Rowell, N.; Ripmeester, J. A.; Renoud, R.; Bian, F.; Zeng, J.; Yu, K. Probing Intermediates of the Induction Period Prior to Nucleation and Growth of Semiconductor Quantum Dots. *Nat. Commun.* **2017**, *8*, 15467.
(25) Zhu, T.; Zhang, B.; Zhang, J.; Lu, J.; Fan, H.; Rowell, N.; Ripmeester, J. A.; Han, S.; Yu, K. Two-Step Nucleation of CdS Magic-Size Nanocluster MSC−311. *Chem. Mater.* **2017**, *29*, 5727−5735.
(26) Wang, Y.; Liu, Y. H.; Zhang, Y.; Wang, F.; Kowalski, P. J.; Rohrs, H. W.; Loomis, R. A.; Gross, M. L.; Buhro, W. E. Isolation of the Magic-Size CdSe Nanoclusters $[(CdSe)_{13}(n\text{-octylamine})_{13}]$ and $[(CdSe)_{13}(oleylamine)_{13}]$. *Angew. Chem., Int. Ed.* **2012**, *51*, 6154−6157.
(27) Muckel, F.; Yang, J.; Lorenz, S.; Baek, W.; Chang, H.; Hyeon, T.; Bacher, G.; Fainblat, R. Digital Doping in Magic-Sized CdSe Clusters. *ACS Nano* **2016**, *10*, 7135−7141.
(28) Eilers, J.; Groeneveld, E.; de Mello Donegá, C.; Meijerink, A. Optical Properties of Mn-Doped ZnTe Magic Size Nanocrystals. *J. Phys. Chem. Lett.* **2012**, *3*, 1663−1667.
(29) Cossairt, B. M.; Juhas, P.; Billinge, S.; Owen, J. S. Tuning the Surface Structure and Optical Properties of CdSe Clusters Using Coordination Chemistry. *J. Phys. Chem. Lett.* **2011**, *2*, 3075−3080.
(30) Bruchez, M., Jr.; Moronne, M.; Gin, P.; Weiss, S.; Alivisatos, A. P. Semiconductor Nanocrystals as Fluorescent Biological Labels. *Science* **1998**, *281*, 2013−2016.
(31) Ming, K.; Kim, J.; Biondi, M. J.; Syed, A.; Chen, K.; Lam, A.; Ostrowski, M.; Rebbapragada, A.; Feld, J. J.; Chan, W. C. Integrated Quantum Dot Barcode Smartphone Optical Device for Wireless Multiplexed Diagnosis of Infected Patients. *ACS Nano* **2015**, *9*, 3060−3074.
(32) Colvin, V. L.; Schlamp, M. C.; Alivisatos, A. P. Light-Emitting Diodes Made from Cadmium Selenide Nanocrystals and a Semiconducting Polymer. *Nature* **1994**, *370*, 354−357.
(33) Lim, S. J.; Zahid, M. U.; Le, P.; Ma, L.; Entenberg, D.; Harney, A. S.; Condeelis, J.; Smith, A. M. Brightness-Equalized Quantum Dots. *Nat. Commun.* **2015**, *6*, 8210.
(34) Nozik, A. J. Quantum Dot Solar Cells. *Phys. E* **2002**, *14*, 115−120.
(35) Yuan, M.; Liu, M.; Sargent, E. H. Colloidal Quantum Dot Solids for Solution-Processed Solar Cells. *Nat. Energy* **2016**, *1*, 16016.
(36) Ekimov, A. I.; Kudryavtsev, I. A.; Efros, A. L.; Yazeva, T. V.; Hache, F.; Schanne-Klein, M. C.; Rodina, A. V.; Ricard, D.; Flytzanis, C. Absorption and Intensity-Dependent Photoluminescence Measurements on CdSe Quantum Dots: Assignment of the First Electronic Transitions. *J. Opt. Soc. Am. B* **1993**, *10*, 100−107.
(37) Nirmal, M.; Brus, L. Luminescence Photophysics in Semiconductor Nanocrystals. *Acc. Chem. Res.* **1999**, *32*, 407−414.
(38) Kucur, E.; Ziegler, J.; Nann, T. Synthesis and Spectroscopic Characterization of Fluorescent Blue-Emitting Ultrastable CdSe Clusters. *Small* **2008**, *4*, 883−887.
(39) Joo, J.; Son, J. S.; Kwon, S. G.; Yu, J. H.; Hyeon, T. Low-Temperature Solution-Phase Synthesis of Quantum Well Structured CdSe Nanoribbons. *J. Am. Chem. Soc.* **2006**, *128*, 5632−5633.
(40) Ouyang, J.; Zaman, M. B.; Yan, F. J.; Johnston, D.; Li, G.; Wu, X.; Leek, D.; Ratcliffe, C. I.; Ripmeester, J. A.; Yu, K. Multiple Families of Magic-Sized CdSe Nanocrystals with Strong Bandgap Photoluminescence via Noninjection One-Pot Syntheses. *J. Phys. Chem. C* **2008**, *112*, 13805−13811.
(41) Liu, Y.; Zhang, B.; Fan, H.; Rowell, N.; Willis, M.; Zheng, X.; Che, R.; Han, S.; Yu, K. Colloidal CdSe 0-Dimension Nanocrystals and Their Self-Assembled 2-Dimension Structures. *Chem. Mater.* **2018**, *30*, 1575−1584.

DOI: 10.1021/acs.jpclett.8b01109
J. Phys. Chem. Lett. 2018, 9, 2818−2824